CCS Chemistry

RESEARCH ARTICLE

Received: Apr. 21, 2022 | Accepted: June 29, 2022 | Published: July 20, 2022

Bioinspired Noncyclic Transfer Pathway Electron Donors for Unprecedented Hydrogen Production

Jing Liu[1†], Chao Wang[1†], Wenbei Yu[1], Heng Zhao[1], Zhi-Yi Hu[1,2], Fu Liu[3], Tawfique Hasan[4], Yu Li[1,2*], Gustaaf Van Tendeloo[1,2,5], Can Li[6*] & Bao-Lian Su[1,7*]

[1]State Key Laboratory of Advanced Technology for Materials Synthesis and Processing, Wuhan University of Technology, 430070 Wuhan, [2]Nanostructure Research Centre (NRC), Wuhan University of Technology, 430070 Wuhan, [3]School of Materials Science and Engineering, Zhejiang University, 310027 Hangzhou, [4]Cambridge Graphene Centre, University of Cambridge, Cambridge CB3 0FA, [5]EMAT (Electron Microscopy for Materials Science), University of Antwerp, B-2020 Antwerp, [6]State Key Laboratory of Catalysis, Dalian Institute of Chemical Physics, 116023 Dalian, [7]Laboratory of Inorganic Materials Chemistry (CMI), University of Namur, B-5000 Namur

**Corresponding authors: yu.li@whut.edu.cn; canli@dicp.ac.cn; baoliansu@whut.edu.cn; bao-lian.su@unamur.be; †J. Liu and C. Wang contributed equally to this work.*

Cite this: *CCS Chem.* **2023**, 5, 1470–1482
DOI: 10.31635/ccschem.022.202202071

Electron donors are widely exploited in visible-light photocatalytic hydrogen production. As a typical electron donor pair and often the first choice for hydrogen production, the sodium sulfide-sodium sulfite pair has been extensively used. However, the resultant thiosulfate ions consume the photogenerated electrons to form an undesirable pseudocyclic electron transfer pathway during the photocatalytic process, strongly limiting the solar energy conversion efficiency. Here, we report novel and bioinspired electron donor pairs offering a noncyclic electron transfer pathway that provides more electrons without the consumption of the photogenerated electrons. Compared to the state-of-the-art electron donor pair Na_2S-Na_2SO_3, these novel Na_2S-NaH_2PO_2 and Na_2S-$NaNO_2$ electron donor pairs enable an unprecedented enhancement of up to 370% and 140% for average photocatalytic H_2 production over commercial CdS nanoparticles, and they are versatile for a large series of photocatalysts for visible-light water splitting. The discovery of these novel electron donor pairs can lead to a revolution in photocatalysis and is of great significance for industrial visible-light-driven H_2 production.

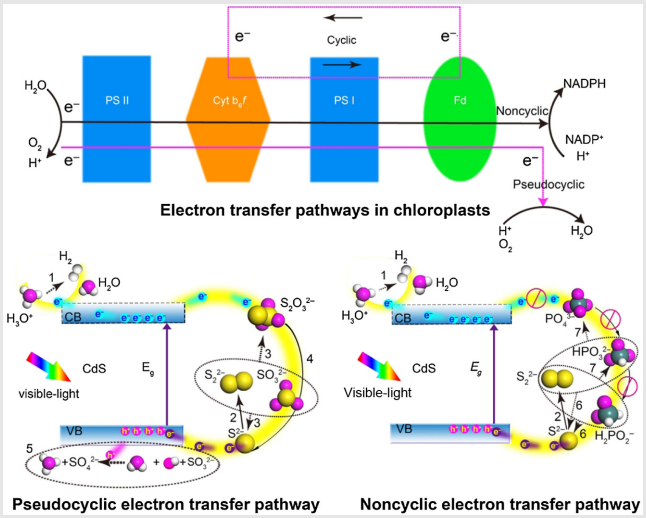

Keywords: noncyclic electron transfer, Na_2S-NaH_2PO_2, Na_2S-$NaNO_2$, electron donor pairs, photocatalytic H_2 production

DOI: 10.31635/ccschem.022.202202071
Citation: *CCS Chem.* **2023**, 5, 1470–1482
Link to VoR: https://doi.org/10.31635/ccschem.022.202202071

Introduction

Photocatalysis based on solar energy-derived H_2 production using semiconductors has been identified as a green, low-cost, and sustainable approach.[1-4] One intrinsic factor for photocatalysis is the transport of the excited electrons, which significantly influences the performance of the photocatalytic H_2 production. In a natural photosynthesis process, three types of electron transfer pathways, occurring via noncyclic, cyclic, and pseudocyclic routes, play a pivotal role.[5] Scheme 1a illustrates the three modes of electron transport. In the *noncyclic* photophosphorylation, two electrons from the water molecule follow a noncyclic electron transfer pathway (NCETP) and are transferred from Photosystem II (PSII) complex to Photosystem I (PSI) complex. Then, the highly excited electrons pass on to ferredoxin-NADP$^+$ (nicotinamide adenine dinucleotide phosphate) reductase to produce NADPH (Reduced NADP, the hydrogen donor in a Calvin cycle).[6] In the cyclic electron transfer pathway (CETP), the electrons present in Photosystem I are energized by light captured by the chlorophyll and pass from ferredoxin to cytochrome b_6f (Cyt b_6f) and plastoquinone instead of NADP$^+$ and then to plastocyanin before returning back to PSI chlorophyll. This chain transport produces a modest proton-motive force, providing the energy for the generation of some ATP.[6] In the pseudocyclic photophosphorylation, the terminal electron acceptor is O_2 instead of NADP$^+$, and reactive oxygen species are formed and inactivated with the help of ascorbate (Mehler's reaction). This electron flow is termed a pseudocyclic electron transfer pathway (PCETP).[6] Therefore, *NCETP* is highly beneficial to transfer electrons to NADPH. Such electron transport is greatly desirable and favorable for the photocatalytic H_2 production. On the contrary, CETP and PCETP are not

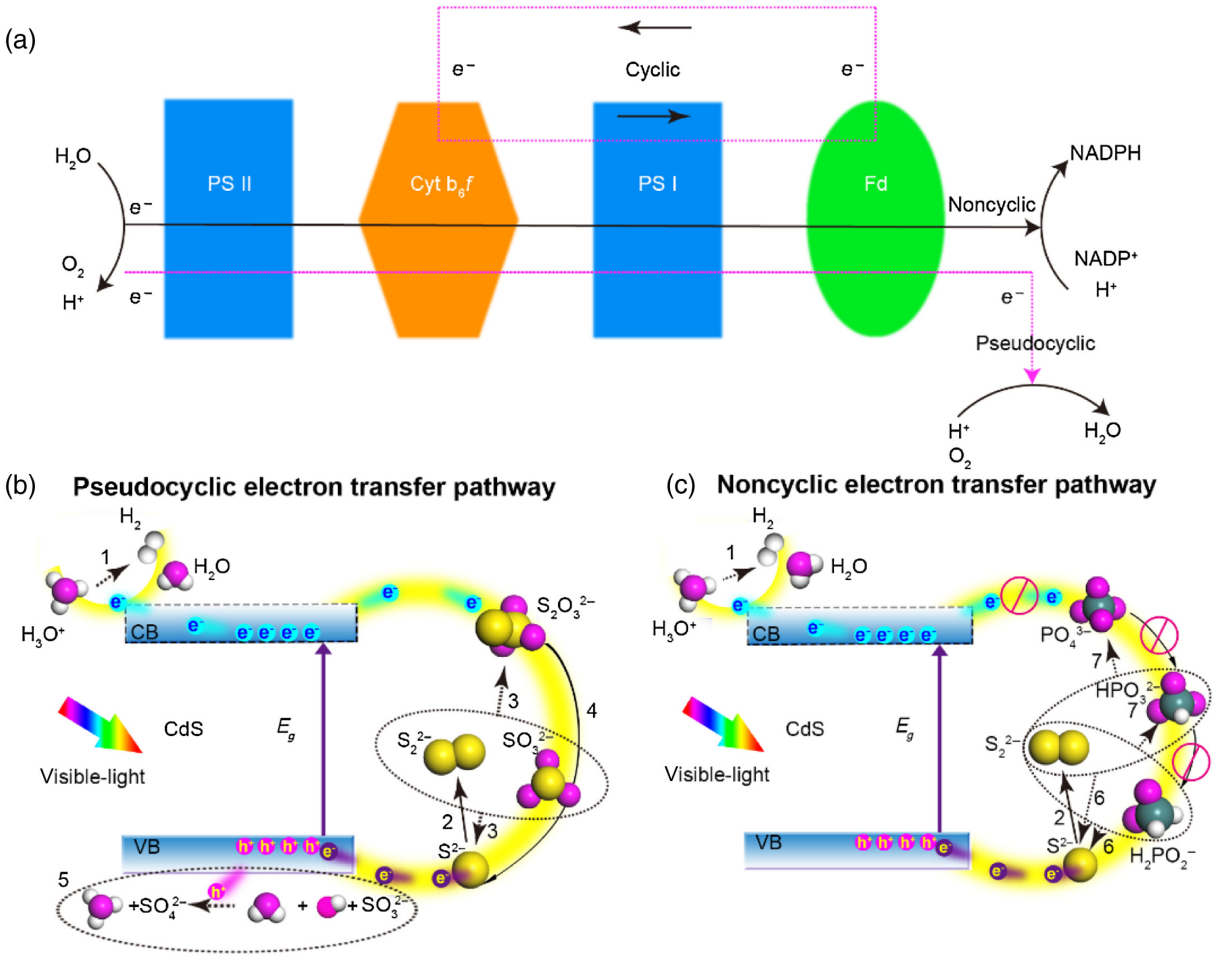

Scheme 1 | *Electron transfer pathway in photoreaction process. (a) The three electron transfer pathways in chloroplasts. (b) PCETP in Na_2S-Na_2SO_3 solution. (c) NCETP in Na_2S-NaH_2PO_2 solution. The blue and purple electrons represent the photogenerated electrons from CdS and donated electrons from sulfion, respectively. The numbers stand for the redox reaction in the process of photocatalysis. The gray, magenta, yellow, and turquoise spheres stand for H, O, S, and P atoms, respectively. The arrows and numbers show the redox reaction process. The red circles mean that the electron transfer is prohibited.*

DOI: 10.31635/ccschem.022.202202071
Citation: *CCS Chem.* **2023**, 5, 1470–1482
Link to VoR: https://doi.org/10.31635/ccschem.022.202202071

favorable for H_2 production due to the consumption of the excited electrons.

Currently, the research effort in photocatalytic H_2 production focuses primarily on the photocatalysts to broaden and/or enhance their light absorption[7–9] and to improve their exciton dissociation by using heterogeneous and hierarchical photocatalysts and cocatalyst/photocatalyst composites.[10–19] Despite the recent substantial achievements by photocatalyst design,[1,20] the utilization of sacrificial electron donor agents[21–23] and expensive noble metals and other substances as cocatalysts[24–26] is indispensable to achieve expected H_2 production performance. Novel sacrificial agents (including organic, low-value chemicals and biomass) and even approaches without sacrificial agents have attracted tremendous attention and are becoming the new development trend in the field of photocatalysis. However, the limited hole-trapping ability, oxidation capabilities, and photocatalytic mechanism still restrain the improvement of photocatalytic performance towards an industrial photocatalytic H_2 production. Although the development of novel electron donor pairs similar to the electrolytes in a natural photosynthesis system still remains a great challenge, it is the most efficient pathway toward a cleaner and more economical industrial photocatalytic H_2 production.

Chalcogenide semiconductor-based artificial photosynthesis,[27] owing to its visible light response, has attracted a great deal of attention for photocatalytic H_2 production. In these systems, the sodium sulfide (Na_2S)-sodium sulfite (Na_2SO_3) couple is always the first choice as the electron donor pair.[28,29] During the photocatalysis process, the H_2 production occurs concomitantly with the oxidation of the sulfide ions (S^{2-}) and the formation of thiosulfate ions ($S_2O_3^{2-}$).[30] The thiosulfate ion being both an oxidant and a reductant is the photogenerated electron acceptor and competes with the hydrogen production.[28] The electrons from donors and photogenerated carriers migrate through a PCETP during the H_2 production process, as shown in Scheme 1b. The major drawback using Na_2S-Na_2SO_3 for sulfide-based semiconductor photocatalytic systems is the undesirable consumption of part of the photogenerated electrons by an intermediate of the electrolytes, leading to reduced H_2 production. It is therefore highly desirable to develop novel electron donor pairs based on a NCETP as the next-generation electrolyte to avoid the PCETP to ensure that their intermediate products only consume the photogenerated holes while keeping the photogenerated electrons for the photocatalysts. This novel approach would significantly improve the efficiency of photocatalytic H_2 production.

Here, we report highly efficient, bioinspired electron donor pairs of sodium hypophosphite (NaH_2PO_2) and sodium nitrite ($NaNO_2$) coupled with Na_2S. The electrons in these novel electron donor pairs follow a NCETP, mimicking the most efficient electron transfer of photoreaction in Photosystem I via a natural photosynthesis process during H_2 production under visible-light irradiation, as shown in Scheme 1c. This electron transfer pathway completely avoids the consumption of photogenerated electrons. These electron donor pairs exclusively consume the photogenerated holes in the photocatalytic H_2 production process and can efficiently ensure carrier transfer and can significantly boost the average H_2 production. When Na_2S-NaH_2PO_2 is used, the average H_2 production rate using commercial cadmium sulfide nanoparticles (C-CdS-NPs) as model photocatalyst can reach as high as ~12.4 $mmol \cdot h^{-1} \cdot g^{-1}$, >3 times higher than that using the state-of-the-art electron donor pair Na_2S-Na_2SO_3. This value is also far superior to those of a large series of transition metal sulfide-based photocatalysts reported in the literature, such as pristine CdS,[30] Pt-CdS,[31] Ni-CdS,[31] WS_2/Graphene-CdS,[32] CdS/L-Histidine,[33] CdS nanoparticles/CdS nanosheets,[34] and CdS nanocubes,[35] with or without cocatalysts. The threshold value of the transient photocurrent of C-CdS-NPs reaches an outstanding value of ~72.6 μA cm^{-2} after the first 50s before stabilizing at ~67.5 μA cm^{-2} after 1000s visible-light irradiation in the Na_2S-NaH_2PO_2 solution. This is 34~36 times higher than that generated by C-CdS-NPs in a Na_2S-Na_2SO_3 solution (~2.0 μA cm^{-2}). Both the time-averaged apparent quantum yield ($\overline{\Phi_A(450)}$) and the photocatalytic activity using the same commercial C-CdS-NP photocatalyst under 450 nm monochromatic light with the Na_2S-NaH_2PO_2 electron donor pair are ~2.9 times higher than those with Na_2S-Na_2SO_3. This work, using the strategy to move from PCETP to a NCETP, demonstrates that these newly discovered bioinspired electron donor pairs can lead to an outstanding performance in the visible-light photocatalytic H_2 production by preventing undesirable photogenerated electron consumption and offering a high charge transfer efficiency on the semiconductor/electrolyte interface and a highly available quantity of donated electrons. The discovery of these NCETP electron donor pairs can potentially have an enormous impact on photocatalytic H_2 production and artificial photosynthesis and represents a major step towards industrialized photocatalytic H_2 production.

Experimental Methods

Chemicals

All the reagents, C-CdS-NPs, commercial MnS nanoparticles (C-MnS-NPs), $Cd(NO_3)_2 \cdot 4H_2O$, $In_2(NO_3)_2$, and thiourea are purchased from Shanghai Aladdin Industrial Corporation (Shanghai, China). Oxalic acid ($H_2C_2O_4$), aniline, and ethanol are purchased from Sinopharm Chemical Reagent Beijing Corporation (Beijing, China). Polyvinylpyrrolidone (MW = 58,000) is purchased from Sigma-Aldrich (Darmstadt, Germany). Resin and

DOI: 10.31635/ccschem.022.202202071
Citation: *CCS Chem.* **2023**, 5, 1470–1482
Link to VoR: https://doi.org/10.31635/ccschem.022.202202071

hardener are purchased from Solaronix Corp. (Aubonne, Switzerland).

Synthesis of CdS nanowires

The CdS nanowires are synthesized by the solvothermal method. 1 mmol cadmium diethyldithiocarbamate is dissolved in a mixture of 30 mL ethylene glycol and 30 mL ethylenediamine. The resultant solution is transferred into a 100 mL Teflon-lined stainless steel autoclave, which is sealed and heated at 180 °C for 24 h and then cooled to room temperature. The obtained bright yellow precipitates are purified several times with distilled water and ethanol. Finally, CdS nanowires are obtained after them in an oven at 60 °C for 12 h in air.

Synthesis of polyaniline@CdS (PANI@CdS) core-shell nanospheres

The PANI@CdS core-shell nanospheres are synthesized as follows[36]: 1.4 mmol porous CdS nanospheres are dispersed in a 20 mL 0.5 mmol·L^{-1} oxalic acid ($H_2C_2O_4$) aqueous solution. 1.4 mmol aniline is added into the above solution, and the mixture is rapidly stirred for 1 h. Finally, 10 mL 0.5 mmol·L^{-1} $H_2C_2O_4$ aqueous solution including ammonium persulfate initiator is added to the above mixture and further stirred for 6 h at room temperature. The obtained PANI@CdS core-shell nanospheres are filtered and washed several times with distilled water.

Synthesis of $CdIn_2S_4$ microflowers

The $CdIn_2S_4$ microflowers are prepared via the solvothermal method.[37] Briefly, 0.1 mmol $Cd(NO_3)_2{\cdot}4H_2O$, 0.2 mmol $In_2(NO_3)_2$, and 0.4 mmol Thiourea are dissolved in 60 mL distilled water and enclosed in a 100 mL microwavable Teflon container. The microwave-assisted digestion reaction is performed at 300W for 1 h. The precipitate is filtered and washed with distilled water by a sand-core funnel. The $CdIn_2S_4$ microflower product is dried at 40 °C for 12 h in air.

Characterizations

The morphology and microstructure of the samples are observed by field emission scanning electron microscopy (S-4800, HITACHI, Tokyo, Japan). Powder X-ray diffraction patterns are obtained on an X-ray diffractometer (XRD, Bruker D8 Advance) using a Cu Kα irradiation source (λ = 1.54056 Å) at a scan rate of 0.05 ° s^{-1}. High-resolution transmission electron microscopy is carried out on a FEI Tecnai G2 (Hillsboro, Oregon, United States) operated at 200 kV. UV–vis diffused reflectance spectra are obtained on a UV–vis spectrophotometer (UV 2550, Shimadzu, Kyoto, Japan). X-ray photoelectron spectroscopy (XPS) is carried out using a customized X-ray photoelectron spectrometer (ESCALAB 205Xi, Thermo Fisher, Waltham, United States). The ion chromatography (IC) was conducted on a DIONEX Aquion (Dionex Ionpac™ AS22 connected with Dionex IonPac™ AG22, Thermo Fisher, Waltham, United States) with $NaHCO_3$ (1.04 M) and $NaCO_3$ (1.4 M) as the mobile phase at 1.2 mL/min for the reacted solution after 5 h under light irradiation.

Preparation of C-CdS-NPs film working electrode

The working electrodes are prepared as follows[38]: 0.03 mmol C-CdS NPs and 15 μL of 5 wt % Nafion solution are dispersed in 1 mL of 3:1 v/v water/isopropanol mixed solvent (750 μL deionized water, 250 μL isopropanol) by sonication to form a homogeneous slurry. The slurry is spin-coated onto the indium-doped tin oxide (ITO)/glass of 1 cm^2 area. The ITO working electrode is sealed by using an Amosil 4 sealant, which is made by homogeneously mixing 100 weight units of Amosil 4R (resin) and 80 weight units of Amosil 4H (hardener). The curing of the sealing of the ITO electrode at 60 °C takes 6 h.

Theoretical calculation

The theoretical calculations based on density functional theory are performed by the Perdew–Burke–Ernzerhof functional within the generalized gradient approximation. The continuum solvation model is used to construct the aqueous environment. All electrons are treated in the calculation process in which the core electron treatment is not special. The total energy is calculated by the polarization function, and the triple atomic numeric basis sets with a global orbital cutoff of 3.6 Å.

Apparent quantum yield and solar-energy conversion efficiency

The average irradiancy of 450 nm monochromatic light can be calculated by the following formula[39]:

$$\overline{E} = (\overline{E}_{\text{center}}/3) + 2\times(\overline{E_{\text{edge}}}/3)$$

Here, the center irradiancy of 450 nm monochromatic light is 6.64 mW·cm^{-2}, and the edge irradiancy of 450 nm monochromatic light is 1.20 mW·cm^{-2}, $\overline{E}$ is 3.01 mW·cm^{-2}.

The irradiation flux can be calculated by the following formula:

$$P = \overline{E} \times A_R$$

where P is irradiation flux and A_R is the photic area of the reactor which is 38.5 cm^2. Thus, the irradiation flux of 450 nm monochromatic light is 0.116 W. The irradiation area of the reactor is 38.5 cm^2.

$N_P^i(450)$ is the incident photon number of 450 nm monochromatic light. t is photoreaction time, λ is

DOI: 10.31635/ccschem.022.202202071
Citation: *CCS Chem.* **2023**, 5, 1470–1482
Link to VoR: https://doi.org/10.31635/ccschem.022.202202071

wavelength of incident light (4.5×10^{-7} m), h is Planck's constant (6.63×10^{-34} J·s), and c is speed of light (2.25×10^{8} m·s^{-1}) in the water. The incident photon number can be calculated by the following formula:

$$N_P^i(450) = Pt\lambda/(hc)$$

Here, the incident photon number of 450 nm monochromatic light for 1 h is 1.26×10^{21}.

$\overline{R_{H2}(450)}$ is the time-averaged rate of photocatalytic hydrogen production under 450 nm monochromatic light between time t_1 and t_2. R_{H2} is the rate of photocatalytic hydrogen production under 450 nm monochromatic light. Therefore, the time-averaged rate of photocatalytic hydrogen production under 450 nm monochromatic light can be calculated by the following formula:

$$\overline{R_{H2}(450)} = \left(\int_{t_1}^{t_2} R_{H2} \times dt\right)/(t_2 - t_1)$$

Here, the time-averaged rate of photocatalytic hydrogen production of C-CdS NPs is 4.50×10^{-9} mol·s^{-1} in Na_2S-Na_2SO_3 and 1.31×10^{-8} mol·s^{-1} in Na_2S-NaH_2PO_2 under 450 nm monochromatic light.

$\overline{\Phi_A(450)}$ is the time-averaged apparent quantum yield under 450 nm monochromatic light. N_A is Avogadro's constant. It can be calculated by the following formula:

$$\overline{\Phi_A(450)} = [(2 \times \overline{R_{H2}(450)} \times N_A \times t)/N_P^i(450)] \times 100\%$$

Here, the time-averaged apparent quantum yield of C-CdS NPs is 1.55% in Na_2S-Na_2SO_3 and 4.51% in Na_2S-NaH_2PO_2 under 450 nm monochromatic light, respectively.

$\overline{\eta(450)}$ is the time-averaged photon-hydrogen energy conversion efficiency under 450 nm monochromatic light, and ΔG_{H2} is the Gibbs free energy of H_2 (237.1 KJ·mol^{-1}). It can be calculated by the following formula:

$$\overline{\eta(450)} = [(\Delta G_{H2} \times \overline{R_{H2}(450)})/P] \times 100\%$$

Here, the time-averaged photon-hydrogen energy conversion efficiency of C-CdS NPs is 0.92% in Na_2S-Na_2SO_3 and 2.68% in Na_2S-NaH_2PO_2 under 450 nm monochromatic light.

Electrochemical measurement

The cyclic voltammetry (CV) and electrochemical impedance spectroscopy (EIS) properties are investigated in a three-electrode cell on an Autolab PGSTAT 302N electrochemical workstation. The C-CdS-NPs film on ITO/glass, mercuric oxide and a platinum plate are used as the working electrode, the reference electrode, and the counter electrode, respectively. A 300 W Xe lamp (PLS-SXE300C) with a 420 nm cutoff filter is used as the light source. The electrolyte is a Na_2S-Na_2SO_3, Na_2S-NaH_2PO_2, or Na_2S-$NaNO_2$ aqueous solution of 0.35 mmol·L^{-1}. They are bubbled with N_2 for 30 min before the start of each experiment. A flow of N_2 is maintained over the electrolyte during the recording of CV. For the C-CdS-NPs eletrode test, the range of the CV measurement is –1.0 to 1.5 V using 0.5 mmol·L^{-1} Na_2SO_4 aqueous solution as electrolyte at the scan rate of 10 mV·s^{-1}. For the other electrochemical measurements, the range of the CV measurement is –0.4 to +1.4 V, and the scan rate is 10 mV·s^{-1}. For EIS, the applied frequency ranges from 100,000 and 0.01 Hz.

Photocurrent measurement

Photocurrent measurements are carried out on an Autolab PGSTAT 302N electrochemical system in the 0.5 mol·L^{-1} Na_2SO_4 aqueous solution with an applied potential of 0.5 V at room temperature. A Pt plate and an Ag/AgCl (3M KCl) electrode are used as the counter electrode and reference electrode, respectively. A 300 W Xe lamp (PLS-SXE300C, Beijing Perfectlight Science & Technology Co., Ltd., Beijing, China) with 420 nm filter is used as the light source. The working electrodes were irradiated from the back side of the ITO/glass during the measurements.

Photocatalytic activity evaluation

The photocatalytic H_2 production is performed in a top irradiation Pyrex cylindrical vessel reactor. The effective irradiation area for the vessel is ~38.5 cm^2, and the visible-light source is 10 cm away from the Pyrex vessel. Typically, 20 mg photocatalysts are dispersed in 50 mL aqueous solution (or D_2O) containing electron donors by a magnetic stirrer in the Pyrex cylindrical vessel. Then the vessel is connected to a gas circulation system (Beijing Perfectlight Science & Technology Co., Ltd., Labsolar-IIIAG system, Beijing, China). The photocatalyst is irradiated under visible light ($\lambda \geq 420$ nm) with a 300 W Xe lamp (PLS-SXE300C). The reaction temperature is maintained at 20 °C by cooling water during the whole photocatalytic process. The produced H_2 is analyzed by an online thermal conductivity detector gas chromatograph (NaX zeolite column, nitrogen as a carrier gas, Agilent 7890B, California, United States).

Results and Discussion

Electron transfer pathway

CV is first carried out to reveal the redox potential of CdS. The result is presented in Supporting Information Figure S1. It shows that the reduced potential of CdS is –0.14 V, and the oxidized potential is 1.06 V. Then, CV measurment is conducted to show the reducibility of different ions in the state-of-the-art electron donor pair

DOI: 10.31635/ccschem.022.202202071
Citation: *CCS Chem.* **2023**, 5, 1470–1482
Link to VoR: https://doi.org/10.31635/ccschem.022.202202071

Na_2S-Na_2SO_3 (Supporting Information Figure S2a–c) and one of the two proposed electron donor pairs (Na_2S-NaH_2PO_2) (Supporting Information Figure S2d,e). This shows that the sulfide ions (S^{2-}) have the strongest reducibility. The photoreaction process in Na_2S-Na_2SO_3 can be described as follows[28,40]:

$$2H_3O^+ + 2e^- \rightarrow H_2\uparrow + 2H_2O \quad (1)$$

$$2S^{2-} + 2h^+ \rightarrow S_2^{2-} \quad (2)$$

$$S_2^{2-} + SO_3^{2-} \rightarrow S_2O_3^{2-} + S^{2-} \quad (3)$$

$$S_2O_3^{2-} + 2e^- \rightarrow S^{2-} + SO_3^{2-} \quad (4)$$

$$SO_3^{2-} + 2h^+ + OH^- + H_2O \rightarrow SO_4^{2-} + H_3O^+ \quad (5)$$

During the photocatalytic H_2 production process (1), S^{2-} is oxidized by the photogenerated holes to form the intermediate S_2^{2-} (2), which then reacts with SO_3^{2-} to form $S_2O_3^{2-}$ and S^{2-} (3). Consequently, the formed $S_2O_3^{2-}$ can further consume the photogenerated electrons to produce S^{2-} and SO_3^{2-} (4). These redox reactions follow a PCETP as illustrated in Scheme 1b. The consumption of the photogenerated electrons by $S_2O_3^{2-}$ inevitably affects the availability of electrons for photocatalytic H_2 production.

For Na_2S-NaH_2PO_2, as S^{2-} still has a stronger reducibility compared to the hypophosphite ions ($H_2PO_2^-$) and phosphite ions (HPO_3^-) (Supporting Information Figure 2d,e), the first two reactions (1) and (2) are the same as in the photoreaction process of Na_2S-Na_2SO_3. However, the following reactions are quite different. The formed S_2^{2-} here will react with $H_2PO_2^-$ to form HPO_3^{2-} (6), which is further oxidized by S_2^{2-} to give PO_4^{3-} (7):

$$S_2^{2-} + H_2PO_2^- + 3OH^- \rightarrow 2S^{2-} + HPO_3^{2-} + 2H_2O \quad (6)$$

$$S_2^{2-} + HPO_3^{2-} + 3OH^- \rightarrow 2S^{2-} + PO_4^{3-} + 2H_2O \quad (7)$$

Our first-principles calculation shows that the energy loss of the redox reactions of Na_2S-NaH_2PO_2 is 2.67 eV (6) and 2.04 eV (7), respectively, and these processes can occur spontaneously. The IC measurement on the reacted solution for the C-CdS-NPs with Na_2S-NaH_2PO_2 after 5 h light irradiation shows that the concentration of PO_4^{3-} is 11.8 mg/L (Supporting Information Figure S3). As a consequence, these reactions follow a NCETP, similar to the photoreaction in Photosystem I of a natural photosynthesis,[6] avoiding the undesirable consumption of photogenerated electrons as illustrated in Scheme 1c. This significantly boosts the photocatalytic H_2 production rate.

Superior photocatalytic H_2 production performance

The performance of these two electron donor pairs—that is, the state-of-the-art electron donor pair Na_2S-Na_2SO_3 and one of the proposed electron donor pairs, Na_2S-NaH_2PO_2—over the model photocatalyst C-CdS-NPs for photocatalytic H_2 production under visible light ($\lambda \geq 420$ nm) is investigated next. The novel electron donor pair, Na_2S-NaH_2PO_2, leads to an impressive enhancement in the photocatalytic H_2 production activity. As revealed in Figure 1a, C-CdS-NPs with Na_2S-NaH_2PO_2 exhibit a very high photocatalytic activity, with a H_2 production of ~62.0 mmol g^{-1}. This is more than three times higher than that with the electron donor pair Na_2S-Na_2SO_3 (19.4 mmol g^{-1}), underscoring the clear superiority of our strategy. The H_2 evolution rate with Na_2S-NaH_2PO_2 over C-CdS-NPs also shows an exceptional stability in three 5-h cycles under visible light. In comparison, the H_2 production rate for the state-of-the-art Na_2S-Na_2SO_3 over C-CdS-NPs rapidly decreases (Figure 1a), in line with the observations in the literature. The optimization of the molar ratio of Na_2S and NaH_2PO_2 (2:1, 1:1, and 1:2) can further boost the photocatalytic activity (Figure 1b). We found that Na_2S:NaH_2PO_2=1:1 gives the highest photocatalytic H_2 production. More detailed information about the ratio of Na_2S:NaH_2PO_2 will be discussed in our future work.

Moreover, we measured the time-averaged apparent quantum yield ($\overline{\Phi_A(X)}$) and the time-averaged photon-hydrogen energy conversion efficiency ($\overline{\eta(X)}$) of C-CdS-NPs with Na_2S-NaH_2PO_2 using monochromatic light (X = 450, 500, and 550 nm). Figure 1c demonstrates the H_2 production under 450 nm monochromatic light. It shows that C-CdS-NPs with Na_2S-NaH_2PO_2 exhibit a 288% improvement in photocatalytic performance (11.8 mmol·g^{-1} in 5 h) compared to Na_2S-Na_2SO_3 (4.1 mmol·g^{-1} in 5 h). Figure 1d shows that the rate of H_2 production and the apparent quantum yield ($\Phi_A(450)$) of C-CdS NPs with Na_2S-NaH_2PO_2 are 2.6, 2.5, 3.1, 3.0, and 2.9 times higher than those with Na_2S-Na_2SO_3 at every interval hour (Supporting Information Table S1). The time-averaged apparent quantum yield ($\overline{\Phi_A(450)}$) and the time-averaged photon-hydrogen energy conversion efficiency ($\overline{\eta(450)}$) of C-CdS-NPs with Na_2S-NaH_2PO_2 is 4.51% and 2.68%, respectively, both exceeding those with Na_2S-Na_2SO_3 by an unprecedented factor of 291% (Supporting Information Table S2). The ($\overline{\Phi_A(500)}$) and ($\overline{\eta(500)}$) of C-CdS-NPs with Na_2S-NaH_2PO_2 are 1110% and 1133% higher than with Na_2S-Na_2SO_3. The decrease of ($\overline{\Phi_A(550)}$) and ($\overline{\eta(550)}$) with the increase in wavelength indicates that the reaction proceeds via photoabsorption by the catalyst which coincides with the intrinsic absorption of CdS. Compared to the finely designed CdS-based nanostructures with Pt, Ni, WS_2, L-Histidine, and Cd as cocatalysts or special additives using the state-of-the-art electron donor pair Na_2S-Na_2SO_3, the simple C-CdS-NPs with novel Na_2S-NaH_2PO_2 under the same reaction conditions exhibit a significantly higher photocatalytic H_2 production activity (Supporting Information Figure S4). This demonstrates that our proposed electron donor pair is an ideal electrolyte for large-scale visible

DOI: 10.31635/ccschem.022.202202071
Citation: *CCS Chem.* **2023**, 5, 1470–1482
Link to VoR: https://doi.org/10.31635/ccschem.022.202202071

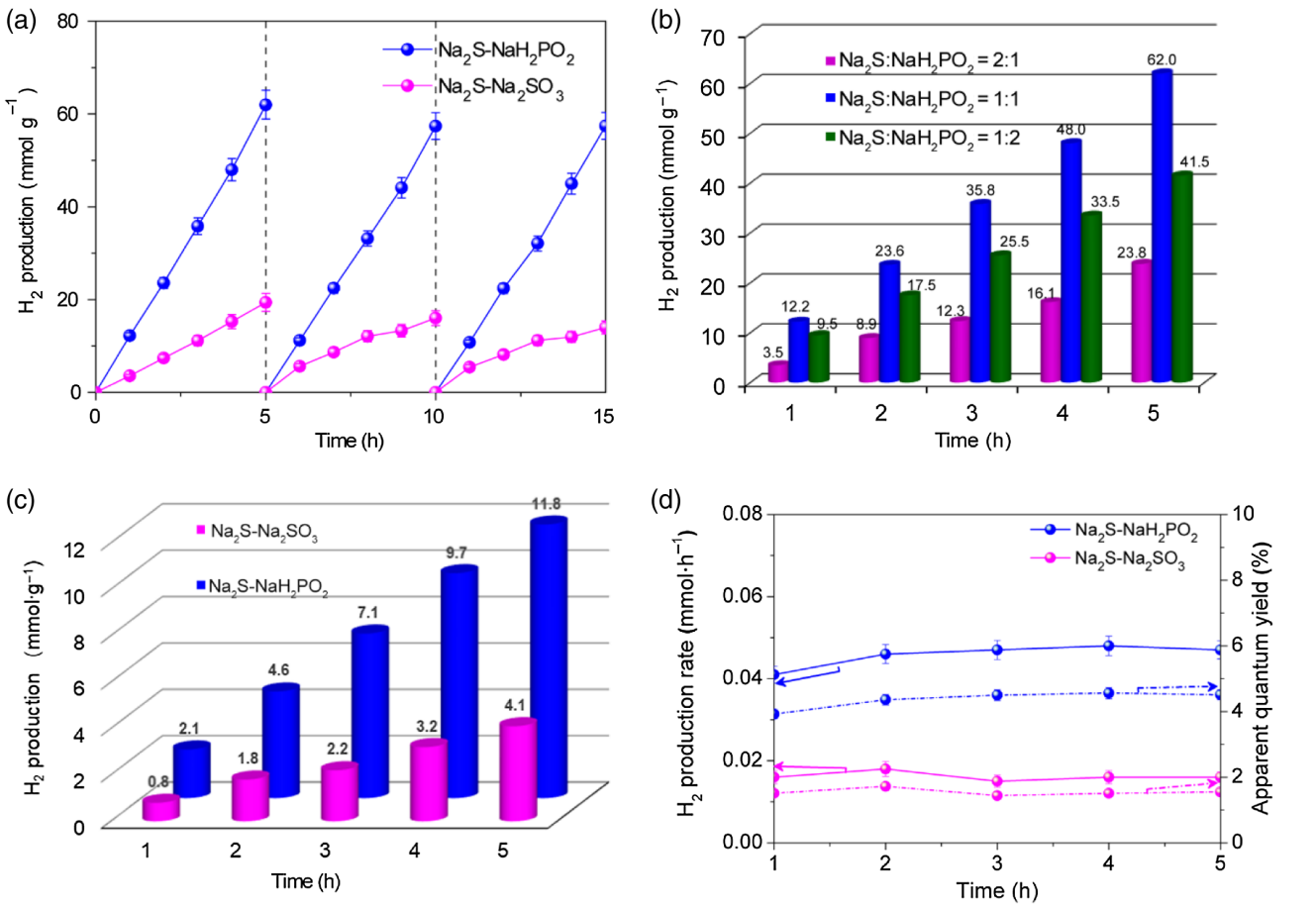

Figure 1 | *Photocatalytic H_2 production. (a) H_2 production under visible light ($\lambda \geq 420$ nm). (b) H_2 production in different molar proportions of Na_2S-NaH_2PO_2 under visible light ($\lambda \geq 420$ nm). (c) H_2 production in Na_2S-Na_2SO_3 and Na_2S-NaH_2PO_2 under monochromatic light (450 nm) and (d) H_2 production rate (solid line) and apparent quantum yield (dashed line) under monochromatic light (450 nm).*

light-driven H_2 production since it significantly outperforms the state-of-the-art.

In the literature, the decrease in H_2 production rate using CdS as photocatalyst is usually attributed to the partially oxidized surface of CdS, which usually leads to the solution turning from faint yellow to black.[41] However, in our experiment, the solution retains the faint yellow of CdS. This suggests that there is no occurrence of photocorrosion. We then investigated the crystallinity phase of the reacted C-CdS-NPs with the two electron donor pairs, that is, novel Na_2S-NaH_2PO_2 and the state-of-the-art NaS_2-Na_2SO_3, by XRD but observed no difference (Supporting Information Figure S5a). The analysis of morphology and crystalline structure of the pristine and reacted C-CdS-NPs by electron diffraction and electron microscopy (Supporting Information Figure S5b–d) also reveals no detectable difference of the reacted C-CdS-NPs after 15 h of visible-light irradiation compared to fresh C-CdS-NPs. The reacted C-CdS-NPs are further analyzed by XPS (Figure 2a,b). The typical peaks of Cd 3d5/2 and S 2p3/2 in the binding energy can be observed at 404.5 and 160.8 eV, respectively. The symmetrical peaks of Cd 3d5/2 and S 2p3/2 indicate that there is no detectable oxidation on the surface of the reacted C-CdS-NPs compared to the pristine samples, consistent with the unchanged color of the solution in the experiment. Therefore, the decrease rate of H_2 production observed is not due to the partial oxidation of CdS with Na_2S-Na_2SO_3. We propose that this is due to the extra consumption of photogenerated electrons, as shown in Scheme 1a. In contrast, no photogenerated electrons in Na_2S-NaH_2PO_2 are consumed by the intermediate products (Scheme 1b), which explains the boost in photocatalytic H_2 production.

Redox capability, charge separation, and transfer

The above results show that Na_2S-NaH_2PO_2 as novel electron donor pair greatly boosts the photocatalytic

DOI: 10.31635/ccschem.022.202202071
Citation: *CCS Chem.* **2023**, 5, 1470–1482
Link to VoR: https://doi.org/10.31635/ccschem.022.202202071

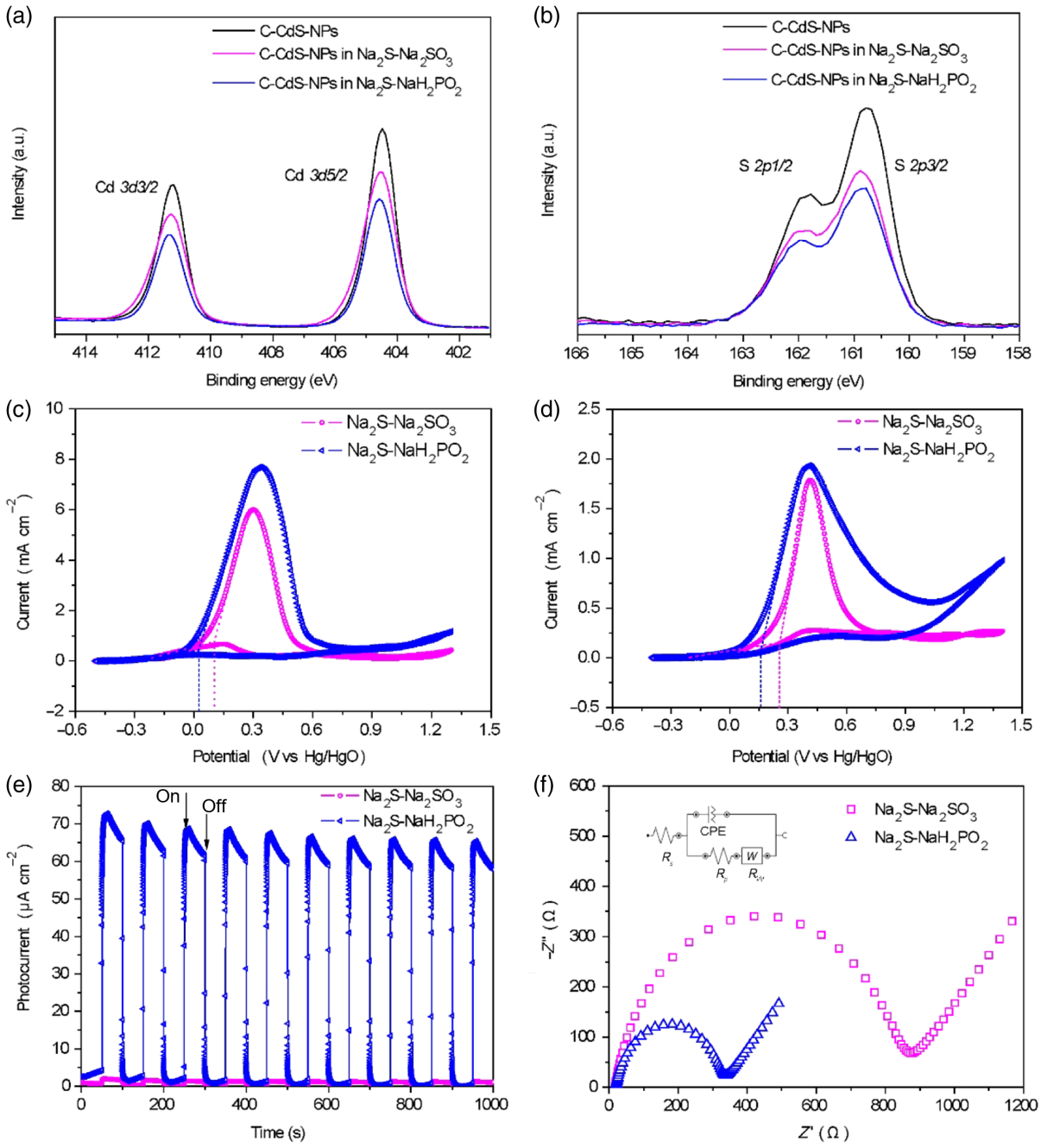

Figure 2 | *Chemical state, photocurrent, and electrochemical studies. XPS spectra of (a) Cd 3d and (b) S 2p. (c) CV curves of glassy carbon electrode (dashed lines show the oxidation potential edge). (d) CV curves of the C-CdS NPs film electrode under visible light (λ ≥ 420 nm). (e) Photocurrent curves and (f) Nyquist plots of C-CdS-NPs in the aqueous solution of Na_2S-Na_2SO_3 and Na_2S-NaH_2PO_2. The inset in (f) shows the equivalent circuit model.*

H_2 production. We next carried out CV tests over a glassy carbon electrode for Na_2S-NaH_2PO_2 and the state-of-the-art NaS_2-Na_2SO_3 electron donor pairs. Figure 2c displays the oxidation edges of the two electron donor pairs. The oxidation edge of the Na_2S-NaH_2PO_2 pair shifts to a more negative potential with an increased oxidation current density. This indicates that Na_2S-NaH_2PO_2 consumes the photogenerated holes more effectively than Na_2S-Na_2SO_3 during the photocatalysis process. To better demonstrate the oxidation reactions of these two different electron donor pairs under visible-light irradiation, a C-CdS-NPs film on ITO/glass as a working electrode is prepared. The result in Figure 2d shows that the Na_2S-NaH_2PO_2 pair has a more negative oxidation edge than Na_2S-Na_2SO_3 on the C-CdS-NPs film. Under the light irradiation, the photogenerated holes will be captured and accumulated on the electrode, which will increase the onset potential. This leads to a more positive

DOI: 10.31635/ccschem.022.202202071
Citation: *CCS Chem.* **2023**, 5, 1470–1482
Link to VoR: https://doi.org/10.31635/ccschem.022.202202071

oxidation edge observed for the Na_2S-NaH_2PO_2 pair. This further proves that Na_2S-NaH_2PO_2 consumes the photogenerated holes more efficiently than Na_2S-Na_2SO_3, leading to a more efficient exciton dissociation and a significantly improved photocatalytic H_2 production.

The higher exciton dissociation efficiency of C-CdS-NPs with Na_2S-NaH_2PO_2 in the aqueous solution compared to Na_2S-Na_2SO_3 was further supported by the photocurrent response. Figure 2e shows that 420–800 nm unpolarized excitation induces a photocurrent response of C-CdS-NPs at an applied potential of 0.5 V in the electron donor aqueous solution. The formation of a semiconductor electrolyte interface (SEI) in dark conditions leads to an interfacial band bending in C-CdS-NPs, as shown in Supporting Information Figure S6a. During photon excitation, the equilibrium of the dark reaction is broken to prompt a new one for light reaction via the exciton dissociation at the SEI: the photogenerated holes are captured on the C-CdS-NPs surface by reduced species in the electrolyte, and the photogenerated electrons migrate to the ITO/glass (Supporting Information Figure S6b). The threshold value of the transient photocurrent for C-CdS-NPs in Na_2S-NaH_2PO_2 solution reaches an outstanding value of ~72.6 μA cm^{-2} after the first 50 s and stabilizes at ~67.5 μA cm^{-2} after 1000s visible-light irradiation (Figures 2e and 3b). This is 34~36 times higher than that generated by C-CdS-NPs in a Na_2S-Na_2SO_3 solution (~2.0 μA cm^{-2}; Figures 2e and 3b and Supporting Information Figure S7). As can be seen in the Bode phase plots (Supporting Information Figure S8), the electron lifetime of C-CdS-NPs in a Na_2S-NaH_2PO_2 aqueous solution is much longer than that in the Na_2S-Na_2SO_3 aqueous solution under the same irradiation conditions.[41] These results confirm that Na_2S-NaH_2PO_2 can efficiently promote exciton dissociation of C-CdS-NPs. Supporting Information Figure S9 shows the Nyquist plots of C-CdS-NPs in Na_2S-Na_2SO_3 and Na_2S-NaH_2PO_2 at a light intensity of 1 sun. An equivalent circuit model of the EIS of C-CdS-NPs in aqueous solution of these two electron donor pairs demonstrates a modified Randles circuit consisting of a series of resistance (R_s), charge transfer resistance (R_p), constant phase element (CPE), and mass-transfer resistance (R_w).[42] The enlarged Nyquist plots show that the R_s value of C-CdS-NPs in Na_2S-Na_2SO_3 is 17.3 Ω, very close to that of 19.5 Ω in Na_2S-NaH_2PO_2 (Supporting Information Figure S10). The R_w values of C-CdS-NPs in Na_2S-Na_2SO_3 and Na_2S-NaH_2PO_2 are also very similar. This indicates that the effect of both R_s and R_w of C-CdS-NPs in aqueous solution of these two electron donor pairs on the photocatalytic H_2 production rate can thus be negligible. In contrast, the value of R_P obtained from the semicircular arc is 820 Ω for C-CdS-NPs in the Na_2S-Na_2SO_3 aqueous solution while that for Na_2S-NaH_2PO_2 is significantly reduced to 305 Ω (Figure 2f). This confirms that the much lower charge transfer resistance at the semiconductor/electrolyte interface observed for C-CdS-NPs in Na_2S-NaH_2PO_2 contributes to high-performance photocatalytic H_2 production.

Other novel electron donor pairs

The significance of the bioinspired NCETP electron donor concept for H_2 production is further reinforced by investigating Na_2S-$NaNO_2$ as another novel electron donor pair. The selection of the $NaNO_2$ molecule follows the same strategy as NaH_2PO_2 compared to Na_2SO_3. The CV result shows that the reducibility of NO^{2-} is lower than that of S^{2-}, indicating that it has a similar function as $H_2PO_2^-$ (Supporting Information Figure S2f). The photocurrent generated with C-CdS-NPs in Na_2S-$NaNO_2$ aqueous solution is ~42.5 μA cm^{-2} (Supporting Information Figure S11), 21 times higher than that in the Na_2S-Na_2SO_3 aqueous solution. In addition, the Bode phase (Supporting Information Figure S6) and Nyquist plots (Supporting Information Figure S9) show that Na_2S-$NaNO_2$ prolongs the electron lifetime and decreases the charge-transfer resistance of C-CdS-NPs compared with those of Na_2S-Na_2SO_3. The average photocatalytic activity of C-CdS-NPs with Na_2S-$NaNO_2$ is 1.4 times higher than that with Na_2S-Na_2SO_3 (Figure 3a).

Both Na_2S-NaH_2PO_2 and Na_2S-$NaNO_2$ electron donor pairs following NCETP significantly improve the photocatalytic H_2 production rate. Generally, the higher reduction potential is conducive to boost the photocatalytic H_2 production performance. In this case, the novel Na_2S-$NaNO_2$ electron donor pairs following NCETP are expected to bring a higher enhancement of photocatalytic hydrogen production due to their higher oxidation-reduction potential than Na_2S-NaH_2PO_2 (0.8 and 0.61 V for $NaNO_2$ and NaH_2PO_2, respectively; Supporting Information Figure S2f). However, the average photocatalytic activity of C-CdS-NPs with Na_2S-$NaNO_2$ is 2.7 times lower than that with Na_2S-NaH_2PO_2 (Figure 3a). Therefore, it is necessary to further investigate the photocatalytic mechanism of the bioinspired NCETP electron donor pairs.

Photocatalytic H_2-production mechanism

The photocurrent threshold over C-CdS-NPs with Na_2S-NaH_2PO_2 (~72.6 μA·cm^{-2}) and Na_2S-$NaNO_2$ (~42.5 μA·cm^{-2}) is 36 and 21 times higher than that with Na_2S-Na_2SO_3 (~2.0 μA cm^{-2}). This leads to an average H_2 production rate of C-CdS-NPs in Na_2S-NaH_2PO_2 and in Na_2S-$NaNO_2$ to be 3.7 and 1.4 times higher than that in Na_2S-Na_2SO_3 (Figure 3a,b). And Na_2S-NaH_2PO_2 gives the best result. As the H_2 production is largely influenced by the photogenerated electrons, the different electron donor pairs leading to a different H_2 production reveal the differences in chemical reactions. For Na_2S-Na_2SO_3, as indicated in eqs 1–4, the SO_3^{2-} donates two electrons to react with S_2^{2-} to produce $S_2O_3^{2-}$ and S^{2-} where the

DOI: 10.31635/ccschem.022.202202071
Citation: *CCS Chem.* **2023**, 5, 1470–1482
Link to VoR: https://doi.org/10.31635/ccschem.022.202202071

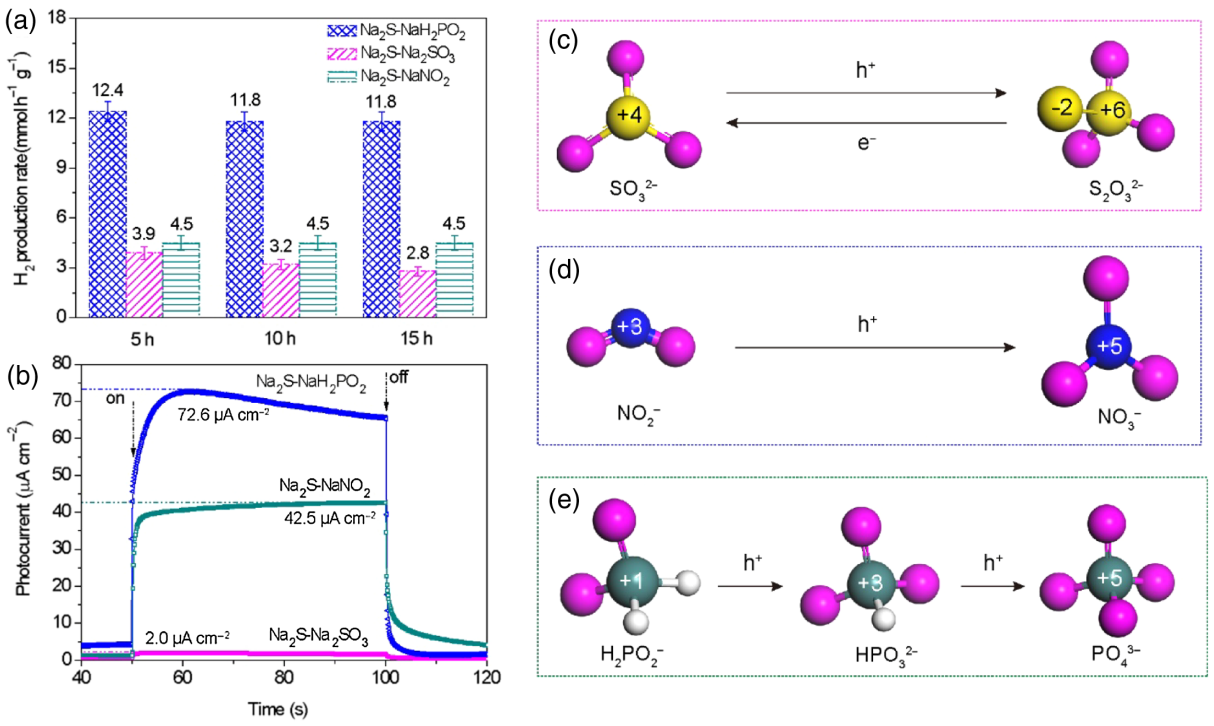

Figure 3 | *H_2 production performance and redox reaction of electron donor pairs. (a) C-CdS-NPs in Na_2S-NaH_2PO_2 (blue grid histograms), Na_2S-Na_2SO_3 (magenta slashed histograms), and Na_2S-$NaNO_2$ (turquoise horizontal histograms). (b) Photocurrent response of the three kinds of electron donor pairs. (c) Na_2SO_3. (d) $NaNO_2$. (e) NaH_2PO_2. The white, magenta, yellow, blue, and turquoise spheres stand for H, O, S, N, and P, respectively.*

S ions in $S_2O_3^{2-}$ are S^{2-} and S^{6+}. In the following reaction, as illustrated in Figure 3c, one S^{6+} in $S_2O_3^{2-}$ consumes two photogenerated electrons and is converted to SO_3^{2-} while S^{2-} remains unreacted. This results in a PCETP and a continuous decrease in H_2 production due to the successive consumption of some of the photogenerated electrons. On the contrary, $H_2PO_2^-$ and NO_2^- only consume the photogenerated holes. In addition, the reactions for $H_2PO_2^-$ and NO_2^- are quite different. NO_2^- only donates two electrons to consume S_2^{2-} to form NO_3^- (Figure 3d). On the other hand, $H_2PO_2^-$ first donates two electrons to consume S_2^{2-} to form HPO_3^{2-}, which gives another two electrons to form PO_4^{3-} (Figure 3e). Thus, there are four donated electrons from $H_2PO_2^-$ while there are only two donated electrons from NO_2^- during the photocatalytic reaction process. We propose that this enables the average photocatalytic H_2 production of C-CdS-NPs in Na_2S-NaH_2PO_2 solution to be 2.7 and 3.7 times higher than those in Na_2S-$NaNO_2$ and in Na_2S-Na_2SO_3, respectively (Figure 3a). These results reveal that more donated electrons by the electron donors can lead to a higher H_2 production performance.

Isotope analysis

We additionally carried out hydrogen isotope analysis to clarify the hydrogen source since the newly discovered Na_2S-NaH_2PO_2 also contains hydrogen. For this, Na_2S-NaH_2PO_2 is dissolved into pure D_2O and H_2O, respectively. We observe only deuterium gas produced in the Na_2S-NaH_2PO_2 deuteroxide solution. On the other hand, no dihydrogen gas is formed in 5 h photoreaction in H_2O during H_2 production (Supporting Information Figure S12). This clearly indicates that the production of hydrogen is from water splitting and not from the electron donor pair Na_2S-NaH_2PO_2.

Universal applicability over sulfide photocatalysts

The photocatalytic H_2 production rates over a large series of sulfide nanostructures: CdS nanowires (CdS-NWs, a typical one-dimensional nanostructure), PANI@CdS core-shell nanospheres (PANI@CdS-NSs, a CdS nanosphere composite), $CdIn_2S_4$ microflowers ($CdIn_2S_4$-MFs, a binary sulfide semiconductor), and C-MnS-NPs (a p-type sulfide semiconductor) with Na_2S-NaH_2PO_2 and Na_2S-Na_2SO_3 are also investigated. Figure 4 shows the H_2 production rates and the corresponding SEM images of these samples. The photocatalytic H_2 production on CdS-NWs, PANI@CdS-NSs, $CdIn_2S_4$-MFs, and C-MnS-NPs with Na_2S-NaH_2PO_2 is 9.1, 5.7, 3.0, and 3.7 times higher than that using the state-of-the-art Na_2S-Na_2SO_3 electron donor pair, respectively (Figure 4). It is known that the

DOI: 10.31635/ccschem.022.202202071
Citation: *CCS Chem.* **2023**, 5, 1470–1482
Link to VoR: https://doi.org/10.31635/ccschem.022.202202071

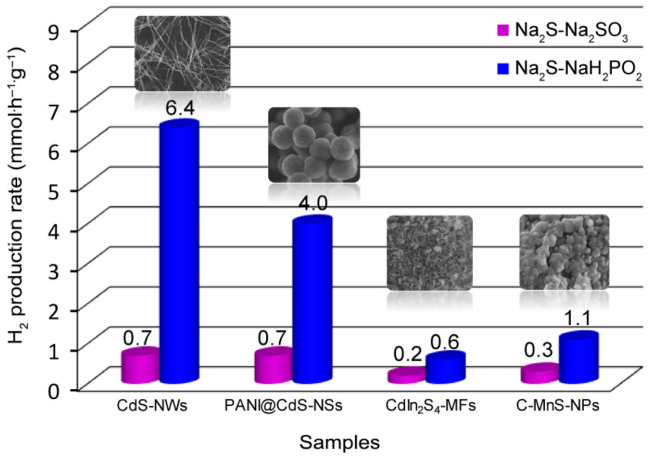

Figure 4 | *Photocatalytic H_2 production rate of various samples. CdS-NWs, PANI@CdS-NSs, $CdIn_2S_4$-MFs, and C-MnS-NPs in Na_2S-Na_2SO_3 (magenta cylinder) and Na_2S-NaH_2PO_2 (blue cylinder) aqueous solutions.*

morphology, structure, crystal, defects, and so on can greatly influence the performance of the photocatalysts. Therefore, the big difference in the photocatalytic H_2 production rate on these sulfides should be closely related to these factors. More detailed studies are being carried out to verify these influencing factors. Our results here clearly confirm that the Na_2S-NaH_2PO_2 electron donor pair with a NCETP has a universal applicability for photocatalytic H_2 evolution over sulfide semiconductors and is clearly superior to the state-of-the-art PCETP electron donor pairs. From both the theoretical point of view and the present results, we envision that these novel electron donor pairs are certainly suitable for no-sulfide semiconductors such as TiO_2, ZnO, and g-C_3N_4 and that this research will be of great significance for industrial visible light-driven H_2 production.

Conclusions

Electron donors play a fundamental role in photocatalytic H_2 production through water splitting. The Na_2S-Na_2SO_3 electron donor pair with a PCETP is currently the most widely used system. We show that such PCETP is detrimental to the photocatalytic property of semiconductors due to the consumption of photogenerated electrons. On the other hand, our proposed bioinspired NCETP electron donor pairs demonstrate a significantly higher photocatalytic H_2 production activity with universal applicability over a large range of sulfide-based photocatalysts. The photocurrent threshold for our Na_2S-NaH_2PO_2 and Na_2S-$NaNO_3$ electron donor pairs over a C-CdS-NP model photocatalyst is 36 and 21 times higher than that using the state-of-the-art Na_2S-Na_2SO_3. This enables their average photocatalytic H_2 production rates to be 3.7 and 1.4 times higher than that using Na_2S-Na_2SO_3. During the photocatalytic reaction process, contrary to the Na_2S-Na_2SO_3 electron donor pair, the intermediate Na_2HPO_3 does not consume the photogenerated electrons but further donates two additional electrons to consume the photogenerated holes. The apparent quantum efficiency via effective exciton dissociation and transportation are also largely improved. We also investigated the different working mechanisms of the *NCETP* electron donor pairs Na_2S-NaH_2PO_3 and Na_2S-$NaNO_2$. We show that four electrons are donated by $H_2PO_2^-$ while only two are donated by NO_2^- for the consumption of the photogenerated holes. The H_2 production activity with Na_2S-NaH_2PO_2 is therefore much higher than that of Na_2S-$NaNO_2$. This strongly suggests that the number of donated electrons has a positive correlation with the H_2 production.

Our work offers a new vision on selecting suitable electron donors via a bioinspired NCETP to strongly enhance and stabilize the H_2 production over a wide range of photocatalysts. Although the design of new photocatalysts and cophotocatalysts is essential, we show that our approach to utilize bioinspired NCETP electron donor pairs could bring a step change in the performance and conversion rate stability, without the use of expensive noble metals as cocatalysts. We strongly believe that our concept of bioinspired NCETP electron donor pairs can usher in a revolution in the field of photocatalysis and be universally applied to other photocatalytic systems. We also envision that the insights gained from this work will facilitate industrial-scale photocatalytic H_2 production.

Supporting Information

Supplemental Information includes Figures S1–S12 and Tables S1 and S2.

Author Contributions

J.L. and C.W. designed the experiments, wrote the original draft of the manuscript, and performed the data analysis. C.W. carried out the synthesis of the materials, H_2 performance testing, and the writing review. W.B.Y. and H.Z. carried out the electrochemical testing. Z.Y.H. carried out transmission electron microscopy characterization and the writing review. F.L. carried out the XPS testing. T.H., G.V.T., and C.L. reviewed the writing and the editing. Y.L. and B.L.S. supervised the project, the writing review, and the editing. All authors discussed and commented on the final version of the manuscript. B.L.S. finalized the manuscript.

DOI: 10.31635/ccschem.022.202202071
Citation: *CCS Chem.* **2023**, 5, 1470–1482
Link to VoR: https://doi.org/10.31635/ccschem.022.202202071

Acknowledgments

This work is financially supported by the National Key R&D Program of China (grant nos. 2016YFA0202602 and 2021YFE0115800), the National Natural Science Foundation of China (grant nos. U20A20122 and 52103285), the Program of Introducing Talents of Discipline to Universities-Plan 111 from the Ministry of Science and Technology and the Ministry of Education of China (grant no. B20002), the "Algae Factory" European Horizon 2020 Program financed by FEDER and Wallonia Region of Belgium (grant no. 1610187), the "DepollutAir" of Interreg V France-Wallonie-Vlaanderen and the Natural Science Foundation of Hubei Province (grant nos. 2018CFB242 and 2020CFB416), the Youth Innovation Research Fund Project of the State Key Laboratory of Advanced Technology for Materials Synthesis and Processing. T.H. acknowledges support from the Royal Academy of Engineering through a Research Fellowship (Graphlex). We also thank Prof. Pierre Van Cutsem, Department of Biology, University of Namur for his advice.

References

1. Wang, H.; Zhang, L.; Chen, Z.; Hu, J.; Li, S.; Wang, Z.; Liu, J.; Wang, X. Semiconductor Heterojunction Photocatalysts: Design, Construction, and Photocatalytic Performances. *Chem. Soc. Rev.* **2014**, *43*, 5234–5244.
2. Tachibana, Y.; Vayssieres, L.; Durrant, J. R. Artificial Photosynthesis for Solar Water-Splitting. *Nat. Photon.* **2012**, *6*, 511–518.
3. Yun, H. J.; Lee, H.; Kim, N. D.; Lee, D. M.; Yu, S.; Yi, J. A Combination of Two Visible-Light Responsive Photocatalysts for Achieving the Z-Scheme in the Solid State. *ACS Nano* **2011**, *5*, 4084–4090.
4. Zhou, H.; Li, X.; Fan, T.; Osterloh, F. E.; Ding, J.; Sabio, E. M.; Zhang, D.; Guo, Q. Artificial Inorganic Leafs for Efficient Photochemical Hydrogen Production Inspired by Natural Photosynthesis. *Adv. Mater.* **2010**, *22*, 951–956.
5. Nobel, P. S. Chapter 5 – Photochemistry of Photosynthesis. In *Physicochemical and Environmental Plant Physiology* (4th ed.); Nobel, P. S., Ed.; Academic Press: San Diego, **2009**; pp 228–275.
6. Allen, J. F. Cyclic, Pseudocyclic and Noncyclic Photophosphorylation: New Links in the Chain. *Trends Plant Sci.* **2003**, *8*, 15–19.
7. Kubacka, A.; Fernández-García, M.; Colón, G. Advanced Nanoarchitectures for Solar Photocatalytic Applications. *Chem. Rev.* **2012**, *112*, 1555–1614.
8. Chen, X.; Liu, L.; Yu, P. Y.; Mao, S. S. Increasing Solar Absorption for Photocatalysis with Black Hydrogenated Titanium Dioxide Nanocrystals. *Science* **2011**, *331*, 746–750.
9. Liu, J.; Zhao, H.; Wu, M.; Van der Schueren, B.; Li, Y.; Deparis, O.; Ye, J.; Ozin, G. A.; Hasan, T.; Su, B.-L. Slow Photons for Photocatalysis and Photovoltaics. *Adv. Mater.* **2017**, *29*, 1605349.
10. Kudo, A.; Miseki, Y. Heterogeneous Photocatalyst Materials for Water Splitting. *Chem. Soc. Rev.* **2009**, *38*, 253–278.
11. Hou, Y.; Laursen, A. B.; Zhang, J.; Zhang, G.; Zhu, Y.; Wang, X.; Dahl, S.; Chorkendorff, I. Layered Nanojunctions for Hydrogen-Evolution Catalysis. *Angew. Chem. Int. Ed.* **2013**, *52*, 3621–3625.
12. Li, J.; Zhan, G.; Yu, Y.; Zhang, L. Superior Visible Light Hydrogen Evolution of Janus Bilayer Junctions via Atomic-Level Charge Flow Steering. *Nat. Commun.* **2016**, *7*, 11480.
13. Li, X.; Yu, J.; Jaroniec, M. Hierarchical Photocatalysts. *Chem. Soc. Rev.* **2016**, *45*, 2603–2636.
14. Li, H.; Bian, Z.; Zhu, J.; Huo, Y.; Li, H.; Lu, Y. Mesoporous Au/TiO_2 Nanocomposites with Enhanced Photocatalytic Activity. *J. Am. Chem. Soc.* **2007**, *129*, 4538–4539.
15. Zong, X.; Yan, H.; Wu, G.; Ma, G.; Wen, F.; Wang, L.; Li, C. Enhancement of Photocatalytic H_2 Evolution on CdS by Loading MoS_2 as Cocatalyst under Visible Light Irradiation. *J. Am. Chem. Soc.* **2008**, *130*, 7176–7177.
16. Han, Z.; Qiu, F.; Eisenberg, R.; Holland, P. L.; Krauss, T. D. Robust Photogeneration of H_2 in Water Using Semiconductor Nanocrystals and a Nickel Catalyst. *Science* **2012**, *338*, 1321–1324.
17. Chang, K.; Mei, Z.; Wang, T.; Kang, Q.; Ouyang, S.; Ye, J. MoS_2/Graphene Cocatalyst for Efficient Photocatalytic H_2 Evolution under Visible Light Irradiation. *ACS Nano* **2014**, *8*, 7078–7087.
18. Liu, J.; Liu, Y.; Liu, N.; Han, Y.; Zhang, X.; Huang, H.; Lifshitz, Y.; Lee, S.-T.; Zhong, J.; Kang, Z. Metal-Free Efficient Photocatalyst for Stable Visible Water Splitting via a Two-Electron Pathway. *Science* **2015**, *347*, 970–974.
19. Regulacio, M. D.; Han, M.-Y. Multinary I-III-VI2 and I2-II-IV-VI4 Semiconductor Nanostructures for Photocatalytic Applications. *Acc. Chem. Res.* **2016**, *49*, 511–519.
20. Hisatomi, T.; Domen, K. Reaction Systems for Solar Hydrogen Production via Water Splitting with Particulate Semiconductor Photocatalysts. *Nat. Catal.* **2019**, *2*, 387–399.
21. Wang, X.; Chen, L.; Chong, S. Y.; Little, M. A.; Wu, Y.; Zhu, W.-H.; Clowes, R.; Yan, Y.; Zwijnenburg, M. A.; Sprick, R. S.; Cooper, A. I. Sulfone-Containing Covalent Organic Frameworks for Photocatalytic Hydrogen Evolution from Water. *Nat. Chem.* **2018**, *10*, 1180–1189.
22. Zhang, Z.; Liu, K.; Feng, Z.; Bao, Y.; Dong, B. Hierarchical Sheet-on-Sheet $ZnIn_2S_4$/g-C_3N_4 Heterostructure with Highly Efficient Photocatalytic H_2 Production Based on Photoinduced Interfacial Charge Transfer. *Sci. Rep.* **2016**, *6*, 19221.
23. Lin, Z.; Du, C.; Yan, B.; Wang, C.; Yang, G. Two-Dimensional Amorphous NiO as a Plasmonic Photocatalyst for Solar H_2 Evolution. *Nat. Commun.* **2018**, *9*, 4036.
24. Lu, Y.; Yin, W.-J.; Peng, K.-L.; Wang, K.; Hu, Q.; Selloni, A.; Chen, F.-R.; Liu, L.-M.; Sui, M.-L. Self-Hydrogenated Shell Promoting Photocatalytic H_2 Evolution on Anatase TiO_2. *Nat. Commun.* **2018**, *9*, 2752.
25. Yue, M.; Wang, R.; Cheng, N.; Cong, R.; Gao, W.; Yang, T. $ZnCr_2S_4$: Highly Effective Photocatalyst Converting Nitrate into N_2 without Over-Reduction under Both UV and Pure Visible Light. *Sci. Rep.* **2016**, *6*, 30992.

DOI: 10.31635/ccschem.022.202202071
Citation: *CCS Chem.* **2023**, 5, 1470–1482
Link to VoR: https://doi.org/10.31635/ccschem.022.202202071

26. Zhao, J.; Zhang, P.; Wang, Z.; Zhang, S.; Gao, H.; Hu, J.; Shao, G. Direct Evidence of Multichannel-Improved Charge-Carrier Mechanism for Enhanced Photocatalytic H_2 Evolution. *Sci. Rep.* **2017**, *7*, 16116.
27. Lu, Q.; Yu, Y.; Ma, Q.; Chen, B.; Zhang, H. 2D Transition-Metal-Dichalcogenide-Nanosheet-Based Composites for Photocatalytic and Electrocatalytic Hydrogen Evolution Reactions. *Adv. Mater.* **2016**, *28*, 1917–1933.
28. Ben-Shahar, Y.; Scotognella, F.; Kriegel, I.; Moretti, L.; Cerullo, G.; Rabani, E.; Banin, U. Optimal Metal Domain Size for Photocatalysis with Hybrid Semiconductor-Metal Nanorods. *Nat. Commun.* **2016**, *7*, 10413.
29. Liu, M.; Chen, Y.; Su, J.; Shi, J.; Wang, X.; Guo, L. Photocatalytic Hydrogen Production Using Twinned Nanocrystals and an Unanchored NiS_x Cocatalyst. *Nat. Energy* **2016**, *1*, 16151.
30. Bao, N.; Shen, L.; Takata, T.; Domen, K. Self-Templated Synthesis of Nanoporous CdS Nanostructures for Highly Efficient Photocatalytic Hydrogen Production under Visible Light. *Chem. Mater.* **2008**, *20*, 110–117.
31. Ran, J.; Gao, G.; Li, F.-T.; Ma, T.-Y.; Du, A.; Qiao, S.-Z. Ti_3C_2 MXene Cocatalyst on Metal Sulfide Photo-Absorbers for Enhanced Visible-Light Photocatalytic Hydrogen Production. *Nat. Commun.* **2017**, *8*, 13907.
32. Xiang, Q.; Cheng, F.; Lang, D. Hierarchical Layered WS_2/Graphene-Modified CdS Nanorods for Efficient Photocatalytic Hydrogen Evolution. *ChemSusChem* **2016**, *9*, 996–1002.
33. Wang, Q.; Lian, J.; Li, J.; Wang, R.; Huang, H.; Su, B.; Lei, Z. Highly Efficient Photocatalytic Hydrogen Production of Flower-like Cadmium Sulfide Decorated by Histidine. *Sci. Rep.* **2015**, *5*, 13593.
34. Shang, L.; Tong, B.; Yu, H.; Waterhouse, G. I. N.; Zhou, C.; Zhao, Y.; Tahir, M.; Wu, L.-Z.; Tung, C.-H.; Zhang, T. CdS Nanoparticle-Decorated Cd Nanosheets for Efficient Visible Light-Driven Photocatalytic Hydrogen Evolution. *Adv. Energy Mater.* **2016**, *6*, 1501241.
35. Zhang, Y.; Han, L.; Wang, C.; Wang, W.; Ling, T.; Yang, J.; Dong, C.; Lin, F.; Du, X.-W. Zinc-Blende CdS Nanocubes with Coordinated Facets for Photocatalytic Water Splitting. *ACS Catal.* **2017**, *7*, 1470–1477.
36. Wang, C.; Wang, L.; Jin, J.; Liu, J.; Li, Y.; Wu, M.; Chen, L.; Wang, B.; Yang, X.; Su, B.-L. Probing Effective Photocorrosion Inhibition and Highly Improved Photocatalytic Hydrogen Production on Monodisperse PANI@CdS Core-Shell Nanospheres. *Appl. Catal. B-Environ.* **2016**, *188*, 351–359.
37. Apte, S. K.; Garaje, S. N.; Bolade, R. D.; Ambekar, J. D.; Kulkarni, M. V.; Naik, S. D.; Gosavi, S. W.; Baeg, J. O.; Kale, B. B. Hierarchical Nanostructures of $CdIn_2S_4$ via Hydrothermal and Microwave Methods: Efficient Solar-Light-Driven Photocatalysts. *J. Mater. Chem.* **2010**, *20*, 6095–6102.
38. Liang, Y.; Li, Y.; Wang, H.; Zhou, J.; Wang, J.; Regier, T.; Dai, H. Co_3O_4 Nanocrystals on Graphene as a Synergistic Catalyst for Oxygen Reduction Reaction. *Nat. Mater.* **2011**, *10*, 780–786.
39. Determination of Energy Conversion Efficiency and Quantum Yield for Hydrogen Production in the Solar Photocatalytic Water Splitting System. General Administration of Quality Supervision, Inspection and Quarantine of the People's Republic of China and National Standards of People's Republic of China, GB/T 26915, PRC, **2011**.
40. Yang, J.; Wang, D.; Han, H.; Li, C. Roles of Cocatalysts in Photocatalysis and Photoelectrocatalysis. *Acc. Chem. Res.* **2013**, *46*, 1900–1909.
41. Rubin, H.-D.; Humphrey, B. D.; Bocarsly, A. B. Role of Surface Reactions in the Stabilization of n-CdS-Based Photoelectrochemical Cells. *Nature* **1984**, *308*, 339–341.
42. Wang, Q.; Moser, J.-E.; Grätzel, M. Electrochemical Impedance Spectroscopic Analysis of Dye-Sensitized Solar Cells. *J. Phys. Chem. B* **2005**, *109*, 14945–14953.

DOI: 10.31635/ccschem.022.202202071
Citation: *CCS Chem.* **2023**, 5, 1470–1482
Link to VoR: https://doi.org/10.31635/ccschem.022.202202071